NASA/CR—2006-213298 AIAA–2004–2814

HiPEP Ion Optics System Evaluation Using Gridlets

John D. Williams, Cody C. Farnell, D. Mark Laufer, and Rafael A. Martinez
Colorado State University, Fort Collins, Colorado

January 2006

The NASA STI Program Office . . . in Profile

Since its founding, NASA has been dedicated to the advancement of aeronautics and space science. The NASA Scientific and Technical Information (STI) Program Office plays a key part in helping NASA maintain this important role.

The NASA STI Program Office is operated by Langley Research Center, the Lead Center for NASA's scientific and technical information. The NASA STI Program Office provides access to the NASA STI Database, the largest collection of aeronautical and space science STI in the world. The Program Office is also NASA's institutional mechanism for disseminating the results of its research and development activities. These results are published by NASA in the NASA STI Report Series, which includes the following report types:

- TECHNICAL PUBLICATION. Reports of completed research or a major significant phase of research that present the results of NASA programs and include extensive data or theoretical analysis. Includes compilations of significant scientific and technical data and information deemed to be of continuing reference value. NASA's counterpart of peer-reviewed formal professional papers but has less stringent limitations on manuscript length and extent of graphic presentations.

- TECHNICAL MEMORANDUM. Scientific and technical findings that are preliminary or of specialized interest, e.g., quick release reports, working papers, and bibliographies that contain minimal annotation. Does not contain extensive analysis.

- CONTRACTOR REPORT. Scientific and technical findings by NASA-sponsored contractors and grantees.

- CONFERENCE PUBLICATION. Collected papers from scientific and technical conferences, symposia, seminars, or other meetings sponsored or cosponsored by NASA.

- SPECIAL PUBLICATION. Scientific, technical, or historical information from NASA programs, projects, and missions, often concerned with subjects having substantial public interest.

- TECHNICAL TRANSLATION. English-language translations of foreign scientific and technical material pertinent to NASA's mission.

Specialized services that complement the STI Program Office's diverse offerings include creating custom thesauri, building customized databases, organizing and publishing research results . . . even providing videos.

For more information about the NASA STI Program Office, see the following:

- Access the NASA STI Program Home Page at ***http://www.sti.nasa.gov***

- E-mail your question via the Internet to help@sti.nasa.gov

- Fax your question to the NASA Access Help Desk at 301–621–0134

- Telephone the NASA Access Help Desk at 301–621–0390

- Write to:
  NASA Access Help Desk
  NASA Center for AeroSpace Information
  7121 Standard Drive
  Hanover, MD 21076

NASA/CR—2006-213298 AIAA–2004–2814

HiPEP Ion Optics System Evaluation Using Gridlets

John D. Williams, Cody C. Farnell, D. Mark Laufer, and Rafael A. Martinez
Colorado State University, Fort Collins, Colorado

Prepared for the
40th Joint Propulsion Conference and Exhibit
cosponsored by AIAA, ASME, SAE, and ASEE
Fort Lauderdale, Florida, July 11–14, 2004

Prepared under Contract NNC04GB20G

National Aeronautics and
Space Administration

Glenn Research Center

January 2006

Acknowledgments

Results of this work were generated under the HiPEP Thruster Development Project being carried out in the On–Board Propulsion and Power Division at NASA Glenn Research Center with direction from Dr. John E. Foster, HiPEP Technical Program Manager, and Dr. George Williams, Senior Research Scientist. Financial support from NASA Glenn Research Center is gratefully acknowledged.

Available from

NASA Center for Aerospace Information
7121 Standard Drive
Hanover, MD 21076

National Technical Information Service
5285 Port Royal Road
Springfield, VA 22100

Available electronically at http://gltrs.grc.nasa.gov

HiPEP Ion Optics System Evaluation Using Gridlets

John D. Williams, Cody C. Farnell, D. Mark Laufer, and Rafael A. Martinez
Colorado State University
Fort Collins, Colorado 80523

Experimental measurements are presented for sub-scale ion optics systems comprised of 7 and 19 aperture pairs with geometrical features that are similar to the HiPEP ion optics system under development within NASA's Project Prometheus. Effects of hole diameter and grid-to-grid spacing are presented as functions of applied voltage and beamlet current. Recommendations are made for the beamlet current range where the ion optics system can be safely operated without experiencing direct impingement of high energy ions on the accelerator grid surface. Measurements are also presented of the accelerator grid voltage where beam plasma electrons backstream through the ion optics system. Results of numerical simulations obtained with the ffx code are compared to both the impingement limit and backstreaming measurements. An emphasis is placed on identifying differences between measurements and simulation predictions to highlight areas where more research is needed. Relatively large effects are observed in simulations when the discharge chamber plasma properties and ion optics geometry are varied. Parameters investigated using simulations include the applied voltages, grid spacing, hole-to-hole spacing, doubles-to-singles ratio, plasma potential, and electron temperature; and estimates are provided for the sensitivity of impingement limits on these parameters.

I. Introduction

The ion current range over which a particular ion optics system can be operated is limited by the onset of destructive direct (i.e., non-charge exchange) ion impingement at both high and low values of ion current per hole (beamlet current).[1] These current limitations can manifest themselves during initial testing of a grid set or after many tens of thousands of hours of operation during a particular mission or life test sequence.

As shown in Fig. 1, when the beamlet current is low, the sheath that separates the discharge chamber plasma from the ion acceleration region is dished upstream to the point where ions are over-focused, their trajectories cross, and, at the limit, ions in the beamlet begin to impinge directly on the downstream edge of the accelerator grid barrel. This low beamlet current condition can occur at the edge of an ion optics system where the plasma density is lower in comparison to the central regions of the thruster. When the beamlet current is high, on the other hand, the sheath is dished less, and the ions can be under-focused to the point where they begin to impinge directly on the upstream side of the accelerator grid. These extreme conditions define the crossover and perveance limits on beamlets that are extracted over the diameter of a given ion optics system. Careful attention must be paid to these limits to prevent direct ion impingement and rapid accelerator grid erosion.

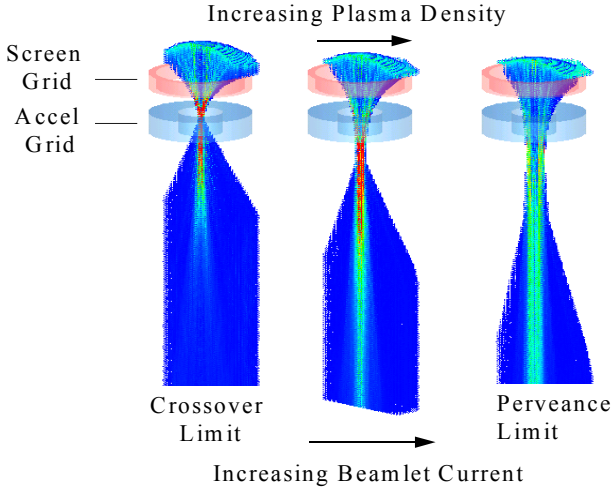

Fig. 1 Simulation results demonstrating perveance and crossover current limitations.

Two consequences exist when direct impingement is allowed to occur. One consequence could cause structural failure of the grid set if the condition were allowed to continue until the webbing between the accel holes was worn through over a finite region of an ion optics system. This concern would only be applicable to extreme operational conditions or very long missions, and is considered to be an unlikely event during in-space operation. The second consequence is more likely and concerns high rates of material being sputtered from the accelerator grid that may re-deposit onto the downstream surface and within the aperture barrel regions of the screen grid. The deposited film on the screen grid can build up to the point where it may crack, de-laminate, and peel from the screen grid sooner than it would if only charge exchange ion impingement was occurring on the accelerator grid. If a flake of the deposited film protrudes into a screen hole, the ion acceleration processes near the screen electrode will be strongly affected and additional ions may be directed into and erode the accelerator grid.[2] In addition to formation of rouge holes, flakes that span the gap between the accelerator and screen grids can cause recycles to occur, and, if the flakes are large in cross-sectional area, they may require excessive use of grid clearing circuitry.

An equally important operational limit on ion optics systems is the backstreaming limit, which is the voltage magnitude that must be applied to the accelerator grid to prevent beam plasma electrons from backstreaming. Ideally the accelerator grid voltage should be held negative of but as close to this limit as possible. This will ensure that damage due to the small current of charge exchange ions that sputter erode and limit the lifetime of this grid will be minimized. Unfortunately, the backstreaming limit can change as the accelerator grid wears over time or when the beam current is changed, and compromises on selecting the magnitude of the accelerator voltage must be made or power supplies must be flown with adjustable voltage capability. Many factors can affect the backstreaming voltage including aperture geometry, net voltage, and beamlet current.[3] The plasma flow field environment in the ion beam is also an important factor in determining the backstreaming limit, and the onset of backstreaming can be strongly affected by the operational conditions associated with the neutralizer and conductive plasma-bridge that forms between the neutralizer plasma and the beam plasma. During a long mission, the accelerator grid can erode to the point where the voltage limit of the accelerator power supply is no longer adequate to stop electrons from backstreaming. This condition defines one important End of Life (EOL) condition for a thruster/power-supply system.

In this paper, we describe tests on sub-scale ion optics assemblies (gridlets) that were fabricated from Poco graphite to geometries that are being considered for the High Power Electric Propulsion (HiPEP) ion thruster under development at the NASA Glenn Research Center as part of NASA's Project Prometheus.[4] The first section of this paper contains a brief description of the experimental apparatus and procedures used to conduct tests on gridlets. The second section contains results of tests where the impingement and backstreaming limitations on beamlet current were measured over wide ranges of operational and geometrical conditions. The final section presents (1) a comparison between experimental measurements and numerical simulations conducted using ffx[5] and (2) a discussion of the sensitivity of impingement limit currents on geometrical and operational parameters.

II. Gridlet Evaluation Technique

A photograph and sketch of the gridlet test facility and a drawing of gridlet geometry are shown in Fig. 2. Tests were conducted by mounting an assembly comprised of two gridlet electrodes to a ring-cusp discharge chamber. The screen and accelerator gridlets were insulated from one another using standoff insulators and were aligned through the use of precision-placed alignment holes.

The beam voltage applied to the screen gridlet and boosted by the discharge chamber anode power supply (not shown in Fig. 2b) was measured relative to tank ground. It is noted that the inner diameter of the discharge chamber anode is 15 cm and this was much larger than the active diameter of the gridlets tested (~3.6 cm). This was done to ensure that the discharge chamber plasma properties would be uniform over the entire gridlet area, and thereby impose common behavior in all beamlets to allow division of the measured beam current (J_B) by the number of apertures to obtain the per hole or beamlet current (J_b). A ground screen was placed between most of the inactive area of the accelerator grid and the beam plasma to limit the collection of beam plasma ions on the inactive regions of the accelerator gridlet surface. The impingement current collected by the accelerator grid was measured using the ammeter shown in Fig. 2b (labeled J_A) and converted to a per beamlet value (J_{imp}) by dividing the ammeter reading by the number of active accelerator grid apertures.

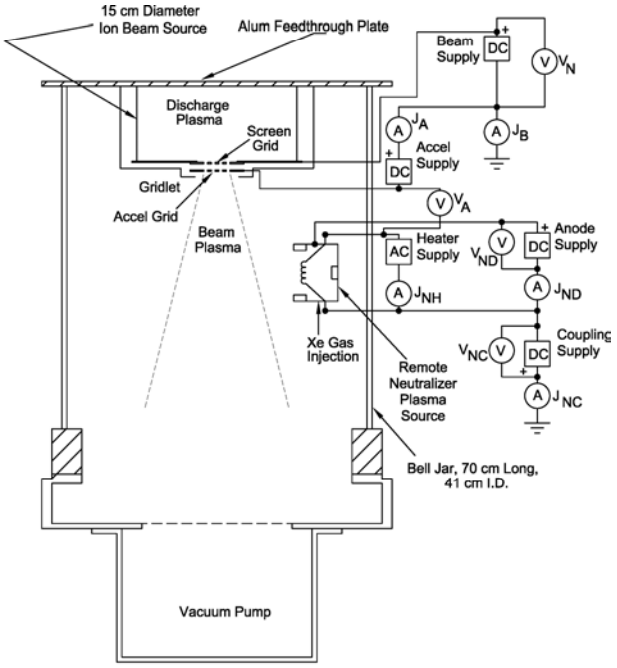

Fig. 2a Sketch of gridlet ion source and neutralizer layout and wiring diagram.

Gridlet test in operation

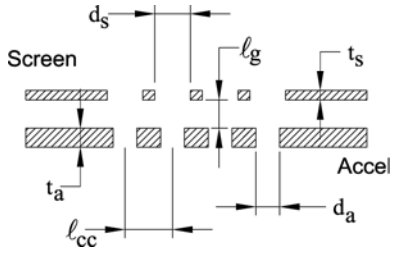

Fig. 2b Gridlet geometry definitions. (See Table 1 for more information)

TABLE 1 HiPEP gridlet geometry and nomenclature.

		Case Study		
Description	**Parameter**	**A**	**B**	**C**
Screen hole diameter	d_s	5.25	5.25	5.25
Screen grid thickness	t_s	3.94	2.62	2.62
Grid gap	ℓ_g	11.36	11.36	11.36
Accel hole diameter	d_a	5.25	5.16	5.25
Accel grid thickness	t_a	3.94	2.95	3.94
Hole-to-hole spacing	ℓ_{cc}	5.34	5.43	5.34
# of holes	H	7 & 19	19	7 & 19

The ion beam was neutralized using a remotely located plasma source. It consisted of a 6-cm diameter, ionization stage that was equipped with a hot filament cathode. The neutralizer plasma source has been operated in a previous study over a wide parameter space of flow rate, discharge power, and coupling bias to investigate the effects these parameters had on gridlet testing.[6] For all of the electron backstreaming characterization presented below, the neutralizer discharge power was set to 3 W, the neutralizer flow rate to 0.1 sccm, and the coupling voltage to -15 V based on results obtained from this earlier study.

The vacuum test facility was 41 cm in diameter and was pumped by a diffusion pump. The base pressure was in the low 10^{-6} Torr range after baking the vacuum chamber for 1 to 2 hours. Xenon flow rates from ~25 to 150 mAeq induced pressures of $2x10^{-5}$ to $3x10^{-4}$ Torr, respectively. These pressures are higher than some large test facilities can achieve with full-sized thrusters. The predominant effect of higher base pressure operation is the observation of higher baseline impingement currents. The baseline impingement current is mostly due to charge-exchange (CEX) ion generation and is proportional to the prevailing beamlet current. As described below, this behavior of CEX being proportional to beamlet current allows one to distinguish between CEX and non-CEX (i.e., direct) impingement currents.

Gridlet testing involved measurement of the beam and accelerator current as the ion source discharge chamber power was varied. The discharge voltage was set to 30 V for most of the tests reported herein. In general, the ion source flow rate was also fixed at the start of a particular test to a value that was ~40 % to 60% larger than that required to operate at the perveance limit of the gridlet under test. However, some testing was conducted at high propellant utilization to study the effects this had on impingement limit data. Gridlet tests were performed over various beam and accelerator voltages to obtain throttling behavior and backstreaming limit data.

Figure 2c contains a sketch of the gridlet geometry and the corresponding nomenclature that will be referred to in this paper. The dimensions of the gridlets are listed in Table 1. Three different case studies were performed on the HiPEP design, and the geometry for the different gridlets are called out by letter (i.e., A, B, and, C) in Table 1. To limit the clutter on the charts presented in the results section of this paper, we have identified all data with their corresponding case study letter.

The ability of an ion optics system to impart a negative potential throughout the beamlet volume near the axial location of the accelerator grid determines its capacity to stop beam plasma electrons from backstreaming into the discharge chamber. The geometry of a typical ion optics aperture set applies boundary conditions that result in an electrostatic potential saddle point being formed near the axial location of the accelerator grid on the beamlet centerline. The saddle point presents the lowest resistance path to electrons on trajectories that could carry them from the beam plasma toward the discharge plasma. The magnitude of the negative voltage that must be applied to the accelerator grid to prevent electron backstreaming, the backstreaming limit, was measured at each beamlet current and grid geometry condition investigated. This was accomplished by (1) setting the accelerator voltage magnitude to a value where no backstreaming occurs, (2) slowing decreasing the accelerator voltage magnitude and simultaneously monitoring the beam current, and (3) reducing the beam current/accelerator voltage data to determine the voltage where the beam current increases to a value 2% above the nominal beam current due to backstreaming electron flow.

III. Results

Experiments were performed where the number of holes, through which ions were extracted, was varied. This was done in sequential tests by attaching two different screen grids (ones with 7 and 19 holes) to a single accelerator grid with 19 holes. The results of these experiments are shown in Figs. 3 and 4, with the impingement current limit data shown in Fig 3 and the backstreaming limit data in Fig. 4. As shown in Fig. 3, the perveance and crossover current limits were very similar for both gridlet sets. Tests have also been conducted with only one hole and significant differences (±25%) were observed relative to the 7 and 19 hole gridlet data due to difficulties in operating the ion source at low flow rates to obtain similar propellant utilization efficiencies used in the 7 and 19 hole tests. It is noted that the ion source would need to be operated with at a flow rate of only 0.05 sccm to match the max propellant utilization we used for the 19 hole gridlet tests. Currently the ion source is not leak tight enough to operate at this low flow rate condition, and, in addition, the flow meter does not have the resolution to indicate flows below ~0.1 sccm accurately.

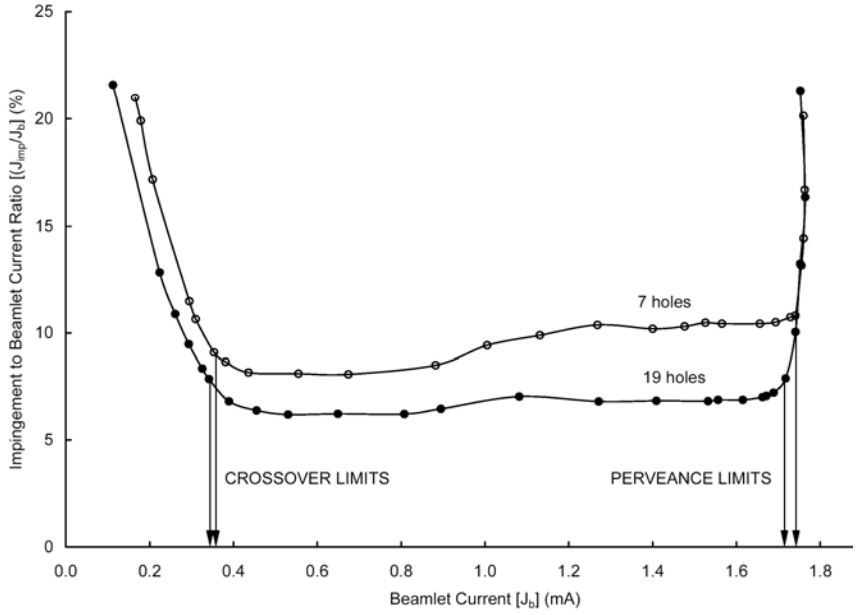

Fig. 3. Effect of changing the number of holes on impingement limit data. (Case A, V_N= 6.5 kV.)

Figure 4 shows the results of the backstreaming tests that were performed on the 7- and 19-hole gridlet sets operated at the same beamlet current where it was observed that the backstreaming limit varied over a 15 V range. This difference is within experimental error, which is mostly due to the voltage increments used to collect the data. Other possible sources of error include differences in the beam plasma properties between the two tests, either because the neutralizer was operated at a slightly different discharge power level and flow rate or because of differences caused by the total beam current that was extracted with 7 and 19 holes gridlets. It is noted that the quick turn-up in the plots at ~430 V are very similar and probably correspond to the initial onset of backstreaming. However, it was felt that more reproducible (albeit less conservative) data are obtained when using the 2% above baseline criteria described in Section II. This is inline with the goal of determining what parameters affect backstreaming limits the most, but may not be adequately conservative for defining full-scale thruster backstreaming limit tests.

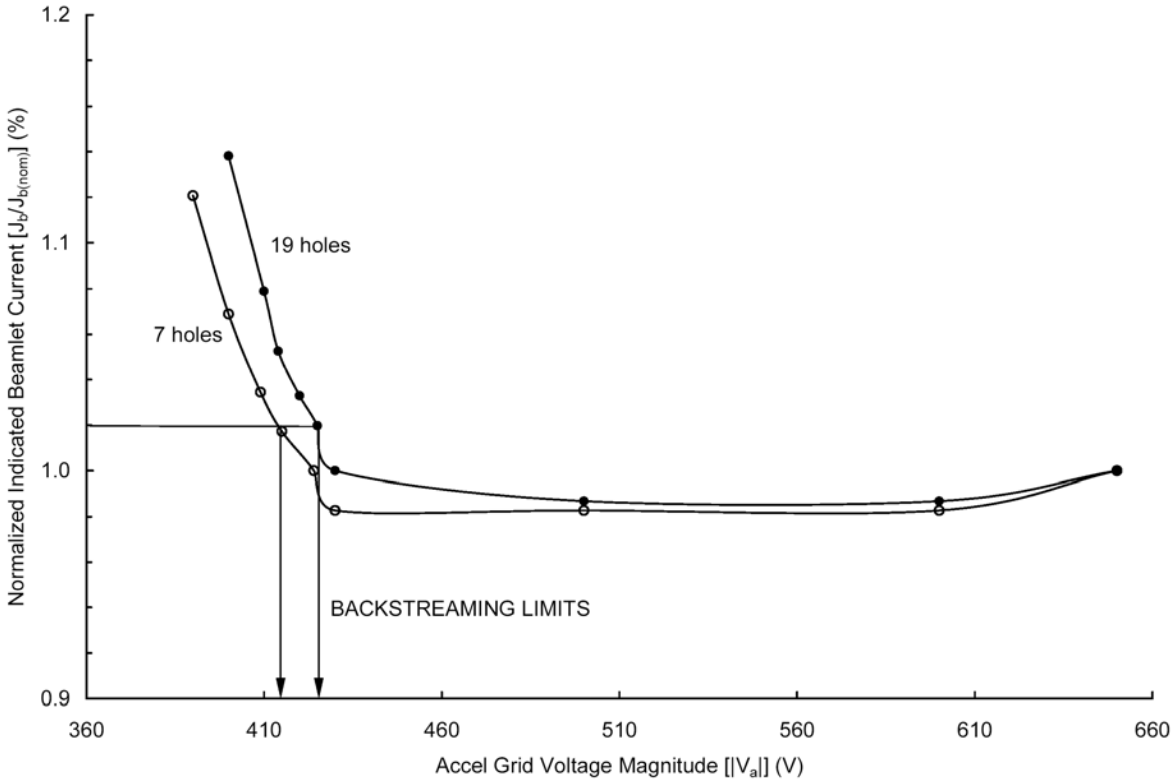

Fig. 4 Effect of changing the number of holes on backstreaming limit behavior at a fixed beamlet current. (Case 5A, V_N = 6.5 kV.)

Several experiments were performed to find the effect of varying the grid spacing on the beamlet current and backstreaming limits. For these experiments, the grids were throttled over a range of net accelerating voltages (V_N) from 5,000 V to 8,000 V. Figure 5 shows impingement limit results obtained at each V_N condition for a Case 5B gridlet). This process was repeated at different grid spacing, and the perveance and crossover limit results are shown in Fig. 6a and 6b. As expected, increasing the spacing resulted in a decrease in the maximum amount of beamlet current that could be extracted at any given net accelerating voltage. In a similar manner, tighter spacing resulted in higher crossover limits. It is interesting to point out that the crossover limits behave in a manner that is similar to the Child-Langmuir dependence on total voltage (i.e., $V_T^{3/2}$), but appear to less sensitive to spacing changes (i.e., less sensitive than ℓ_e^{-2}) . In fact, only the data corresponding to the smallest and largest spacing are shown in Fig. 6b to avoid cluttering up the figure unnecessarily. Figure 6c contains the perveance limit data for the smallest and largest spacing conditions plotted as a function of the total voltage. Curve fits to the data indicate power law dependence on total voltage at values that are also close to the Child-Langmuir law curves. The Child-Langmuir law curves shown in Fig. 6c were obtained using the following equations.

$$J_{b,pl} = \frac{\pi \varepsilon_o}{9} \sqrt{\frac{2zq}{m}} V_T^{3/2} \frac{d_s^2}{\ell_e^2} \quad . \qquad (1)$$

In Eq. (1), $J_{b,pl}$ represents the beamlet current at the perveance limit, ε_o permitivity of free space, q charge on a singly ionized ion, z charge state of ion, m mass of a xenon ion, V_T total voltage difference between the screen and accelerator grids, d_s screen hole diameter, and ℓ_e effective grid gap. The equation for beamlet current was derived from the Child-Langmuir expression for current density by multiplying by the cross-sectional area of a screen hole. The effective ion acceleration length, ℓ_e, was calculated using the following equation.

$$\ell_e = \sqrt{(t_s + \ell_g)^2 + \frac{d_s^2}{4}} \qquad (2)$$

In Eq. (2), t_s represents the screen grid thickness and the other parameters are described above and in Table 2.

Backstreaming data were also obtained during these experiments, and the results are shown in Fig. 7. Again, the results were found to be consistent with expectation (i.e., smaller spacing required larger accelerator voltage magnitudes to stop backstreaming). In addition, the backstreaming limit was observed to be linearly dependent upon the net accelerating voltage. It is noted that all of the data contained in Fig. 7 correspond to beamlet currents that were ~35% of the perveance limit for the given net accelerating voltage condition. This beamlet current corresponded to the point where electron backstreaming would most likely occur.

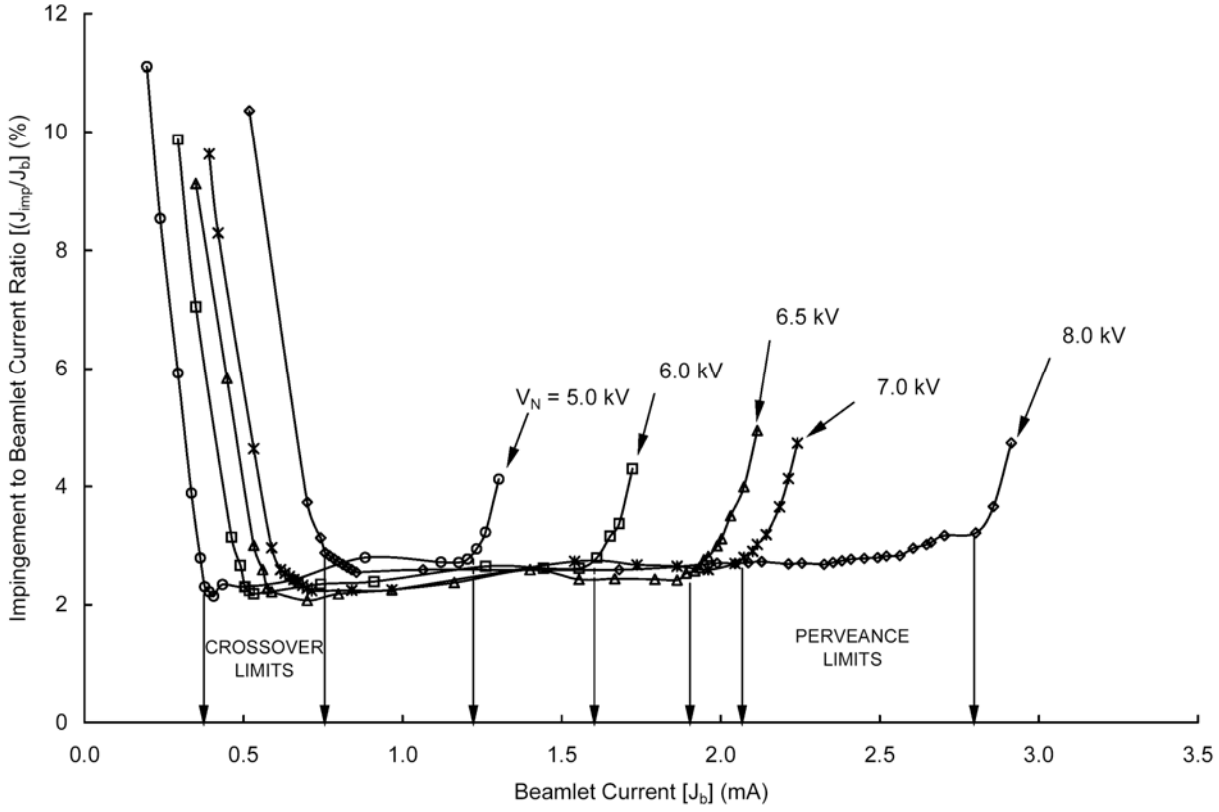

Fig. 5 Effect of changing the net accelerating voltage on impingement limit data. (Case 5B)

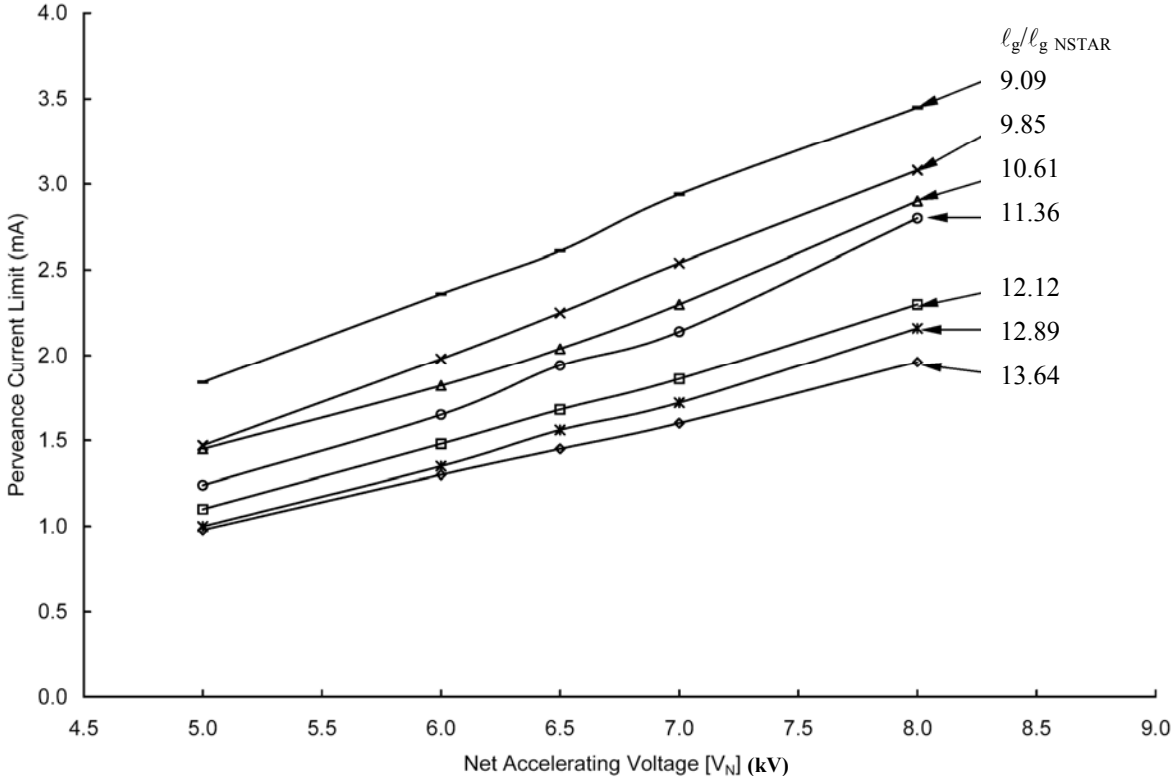

Fig. 6a Perveance current limits for a 7-hole HiPEP gridlet operated at different grid-to-grid spacing. (Case 5B)

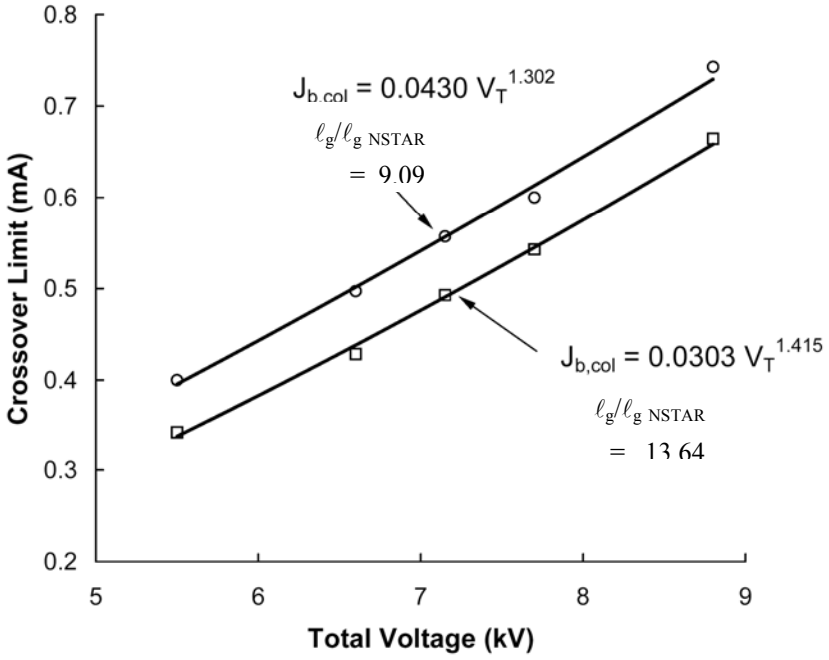

Fig. 6b Crossover current limits for a 7-hole HiPEP gridlet operated at two different spacing conditions. (Case 5B)

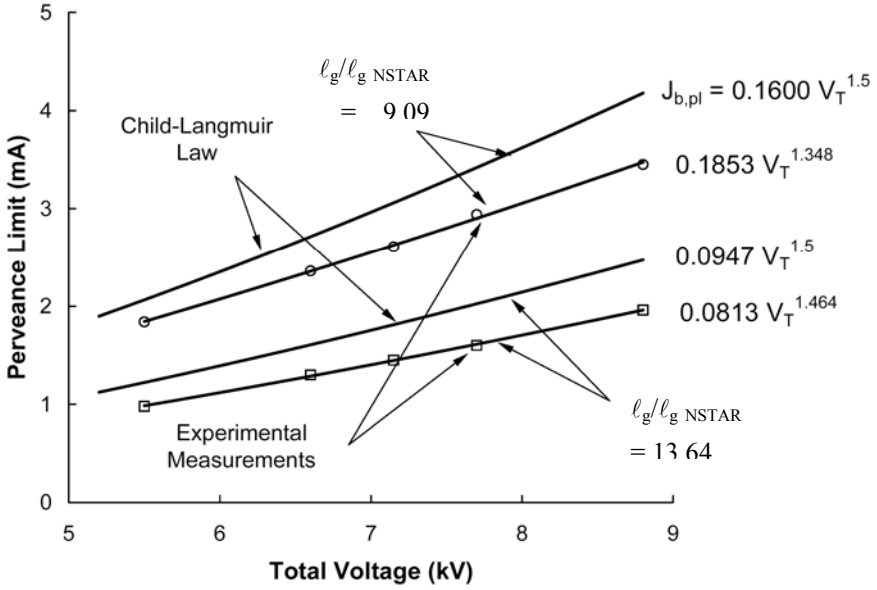

Fig. 6c Perveance limit data from Fig. 6a plotted with Child-Langmuir curves for small and large spacing.

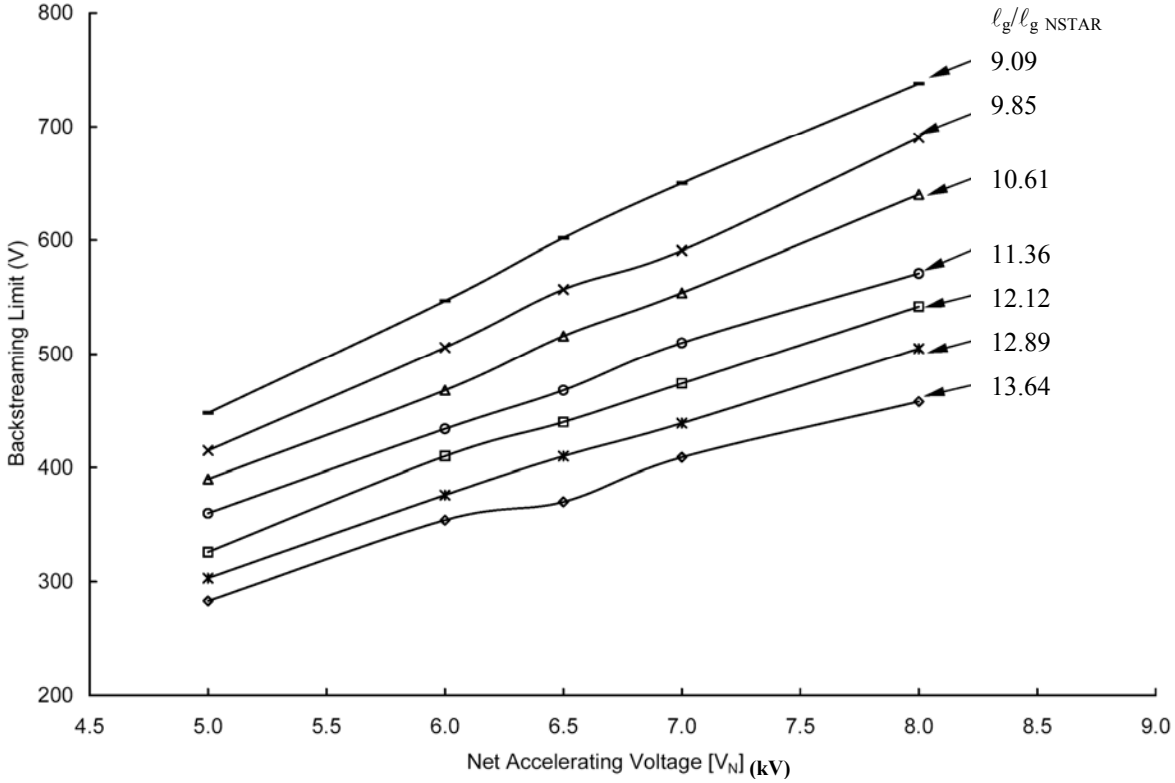

Fig. 7 Backstreaming limit for 7-hole HiPEP gridlets at different grid spacing. (Case 5B)

Figures 8 and 9 show the results of a study in which the accelerator hole diameter was varied. The impingement limit results are shown in Figs. 8a, 8b, and 8c. An increase in the accelerator hole diameter by 36%, which corresponds to an increase in accelerator hole area of about 84%, resulted in a modest 23% increase in the perveance limit (on average as shown in Fig. 8a). Figure 8b shows the crossover limit as a function of total voltage. An increase in the accelerator hole diameter decreased the beamlet current where direct crossover ion impingement

begins to occur. The curve fits in Fig. 8b indicate that the crossover limit follows a power dependence on total voltage that is close to 1.5. The crossover limit data from Figs. 6b and 8b are re-plotted in Fig. 8c after being multiplied by $V_T^{-3/2}$ and by the square-root of the ratio l_e/d_s and the ratio d_a/d_s raised to the 1.5 power. The data cluster about a value of 0.0122 mA/kV$^{3/2}$.

The backstreaming limit data are shown in Fig. 9, where it can be seen that larger accelerator hole diameters lead to the onset of backstreaming at considerably higher accelerator grid voltages. In fact, the initially selected accelerator grid voltage was not adequate to prevent backstreaming in some cases. In this regard it is noted that for the large diameter accelerator hole grids, the impingement experiments were performed at slightly higher accelerator grid voltages to prevent electron backstreaming during the impingement limit measurements. These test results may warrant a more intensive numerical study to determine the tradeoffs of accelerator hole diameter on grid life time and beamlet current limit behavior. It is interesting to note the relatively insensitive dependence of perveance limit on accelerator hole diameter that suggests subtle changes occur in the shape of the screen sheath and beamlet waist at the accelerator grid as the accelerator hole diameter is varied.

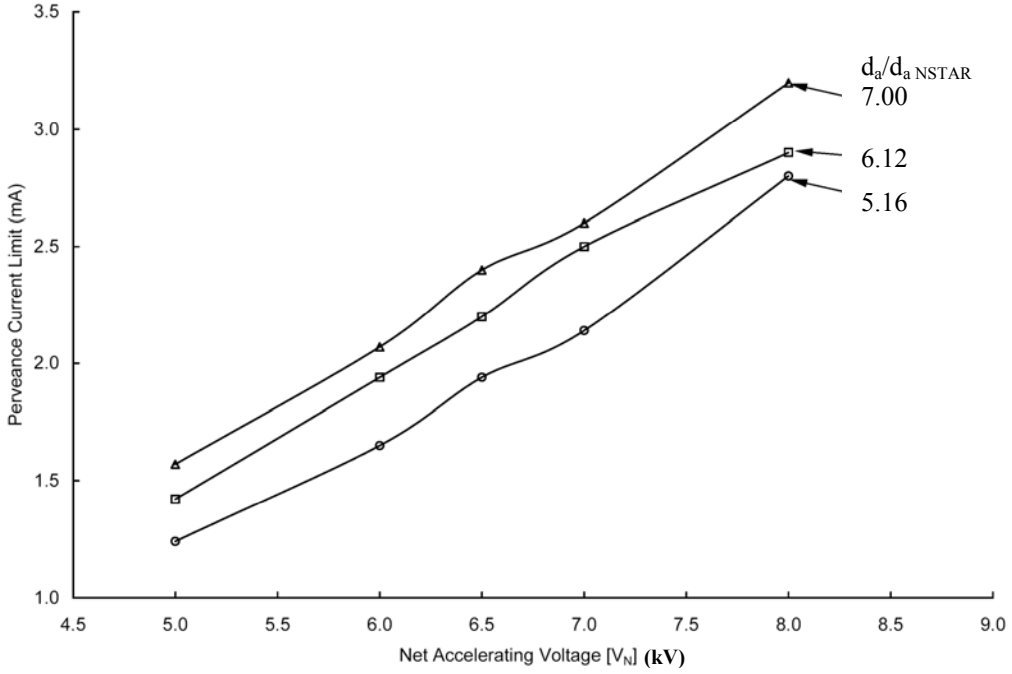

Fig. 8a Perveance limits for 7-hole HiPEP gridlets with different accelerator hole diameters. (Case 5B)

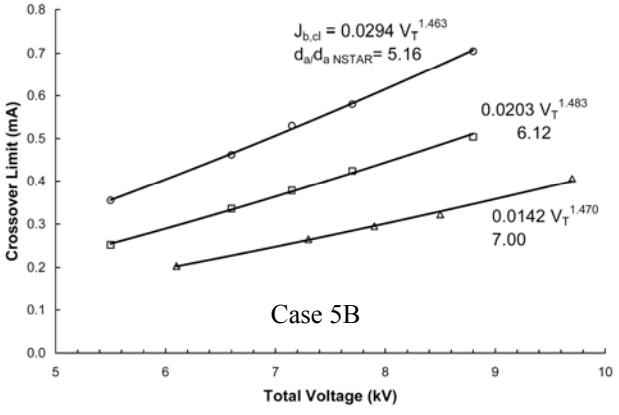

Fig. 8b Crossover limits for different accel hole diameter

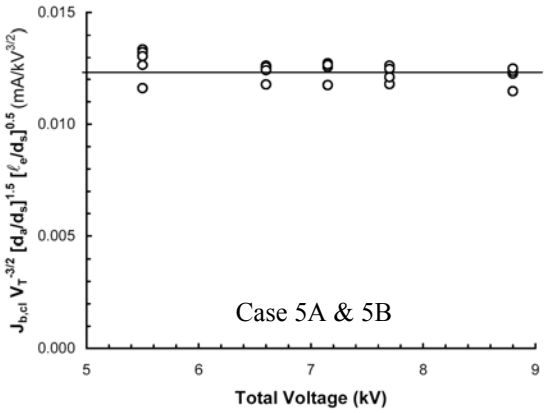

Fig. 8c. Normalization of crossover limit data using experimentally measured sensitivities. (See Table 2)

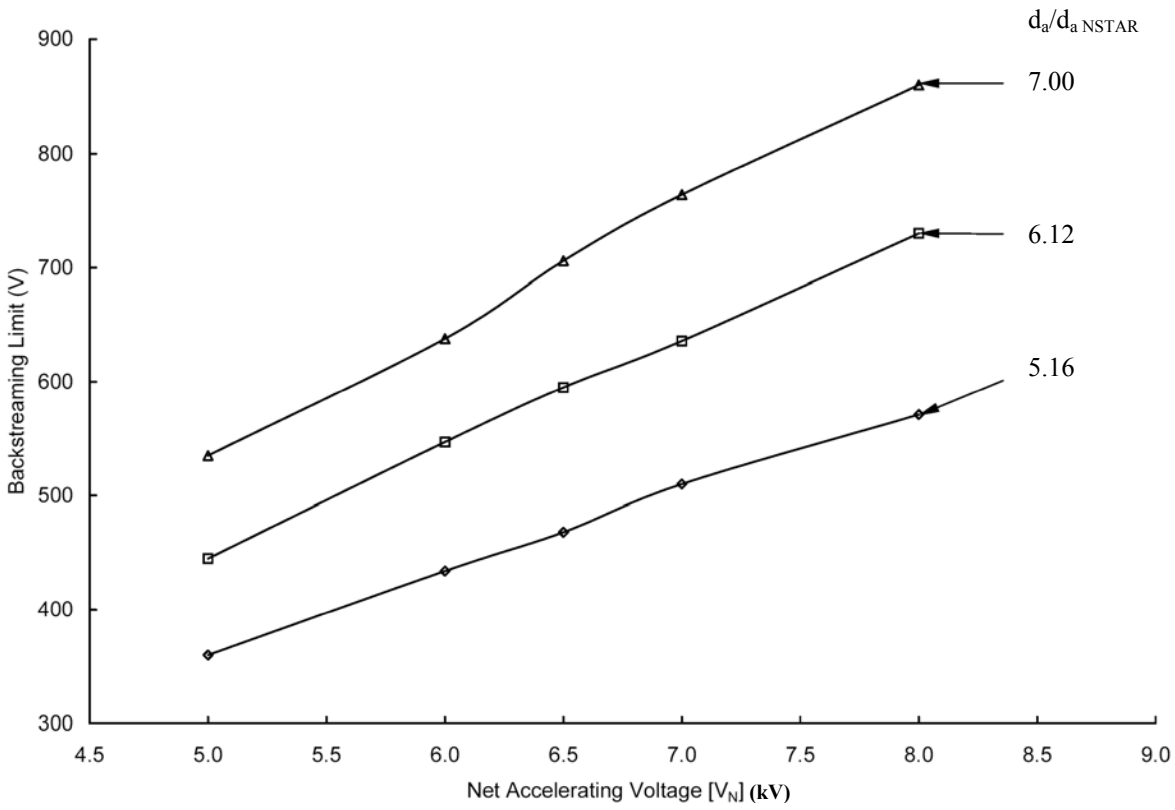

Fig. 9 Backstreaming limit for 7-hole HiPEP gridlets with different accel hole diameters. (Case 5B)

Figure 10 presents impingement current results where the ion source was operated over a range of flow rate and discharge voltage conditions. A wide range of perveance limit currents were observed that, in general, increased with discharge voltage and decreased with flow rate. The main focus of investigation using the ffx code to be presented below was to try to match numerically determined impingement limits with trends observed in impingement limits obtained from gridlet testing. At this point it is noted that the impingement limits determined using the ffx code for HiPEP Case 5A operated at a net voltage (V_N) of 5000 V and an accelerator grid voltage (V_a) of -500 V are low compared to the experimentally determined limits. The experimentally determined crossover limit was at a beamlet current (J_b) of about 0.4 mA, compared with an ffx code crossover limit of about 0.3 mA. The experimentally determined perveance limit ranges between 1.3 and 1.5 mA, depending on the flow rate and discharge voltage, compared to an ffx code perveance limit of about 1.25 mA. (Note that nearly all seven-hole gridlet tests were performed at a moderate flow rate of about 0.35 to 0.45 sccm and with a discharge voltage of 30 V). Flow rate and discharge voltage have an effect on the double-to-single current ratio (J_{++}/J_{+}) and other discharge chamber plasma properties. The discussion presented below summarizes the sensitivity of impingement limit data on various parameters as determined from numerical simulations and gridlet testing.

Figure 11a contains results of numerical simulations that were performed using ffx to determine the crossover and perveance limits for the Case 5C geometry. It is noted that both the perveance and crossover limits increase with total accelerating voltage as observed in experimental data. Only direct (non-charge exchange) impingement currents were used to generate the curves shown in Fig. 11a to clearly identify the beamlet current limits, but the ffx code can determine charge-exchange impingement current as well (e.g., see Fig. 11b).

Figure 12 shows the effects of varying the double-to-single current ratio (J_{++}/J_{+}) on impingement data. The perveance limit is observed to increase with doubles content. To understand this effect consider argon at 40 amu (singly ionized). As predicted by Eq. (1), the argon perveance limit is ~ 1.8 times [i.e., sqrt(131.2/40)] higher than that corresponding to xenon (singly ionized) propellant. Gridlet tests conducted with both Xe and Ar propellants have confirmed this result. Wilbur presents more data on effects of propellant atomic mass on ultra-high Isp, single-hole gridlet systems that are operated on Ar, Kr, and Xe.[7] Next consider a xenon ion source that is comprised of all doubly charged ions. One can think of this source as m=131.2 amu and z=2 or equivalently as m=65.6 amu and z=1.

From the 1-D space-charge-limited equation, one can see that the average ratio of mass-to-charge determines the perveance limit in an electrostatic acceleration scheme. In the extreme case being considered here (i.e., all doubles), the perveance limit would be $2^{1/2}$ times higher than the perveance limit of an ion source that produced only singly charged xenon ions. The gridlet test facility has been recently instrumented with an ExB probe that will enable measurements of the charge state distribution of the beam current, and these measurements will be performed in the near future.

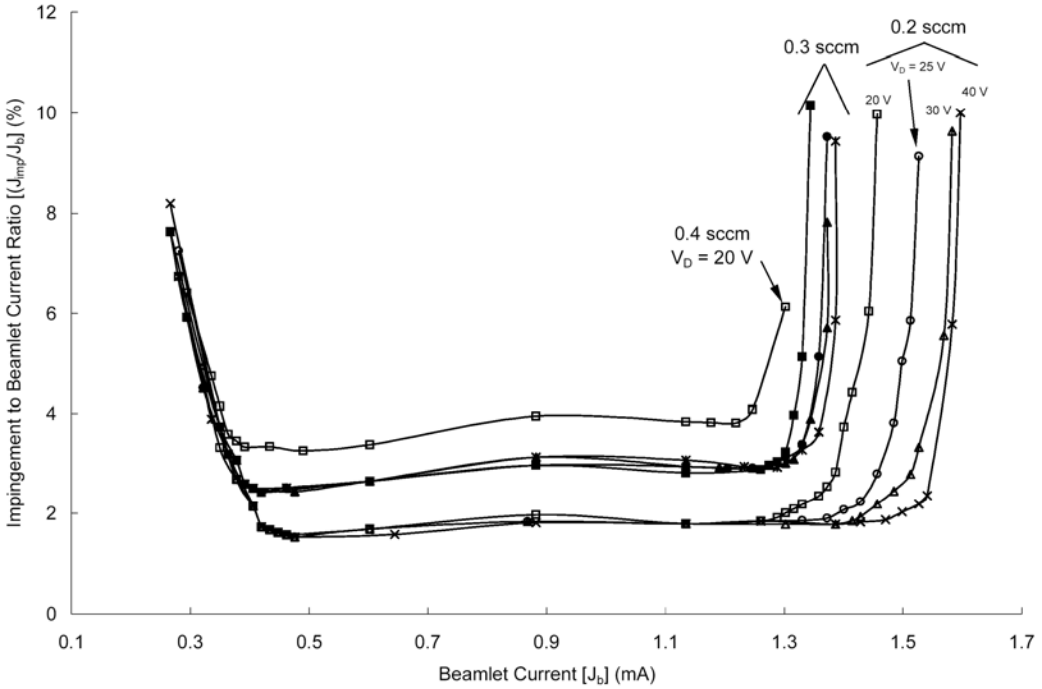

Fig. 10 Seven-hole gridlet data obtained over a range of discharge voltage and flow rate. (Case 5C)

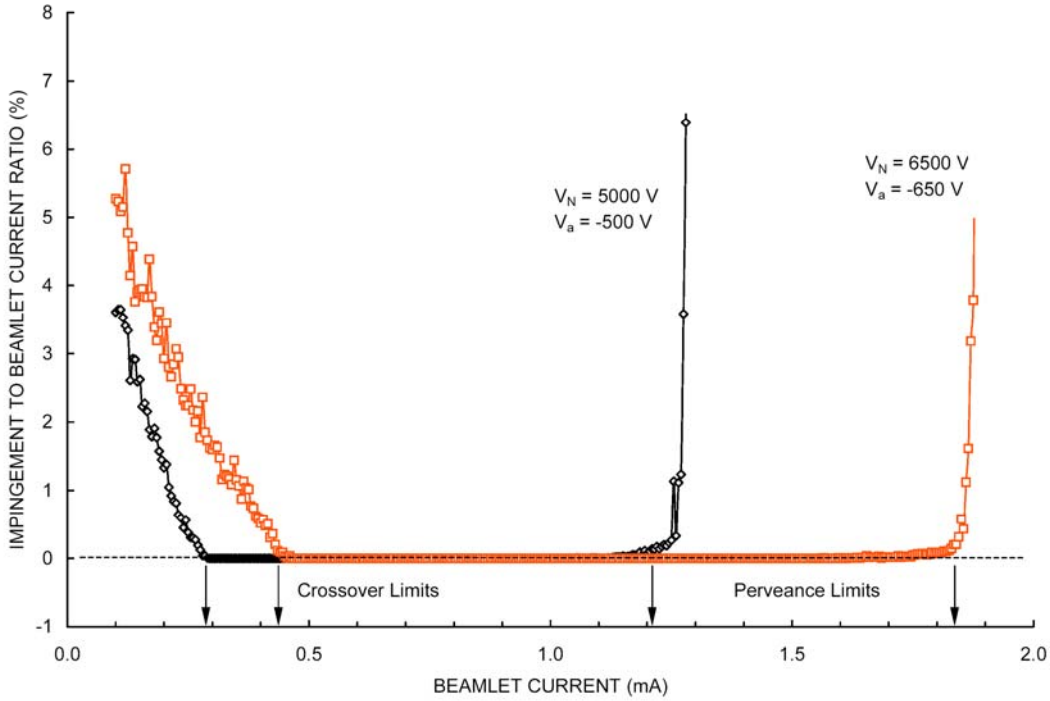

Fig. 11a Typical impingement limit data from ffx at 5 kV and 6.5 kV net accelerating voltages. (Case 5A)

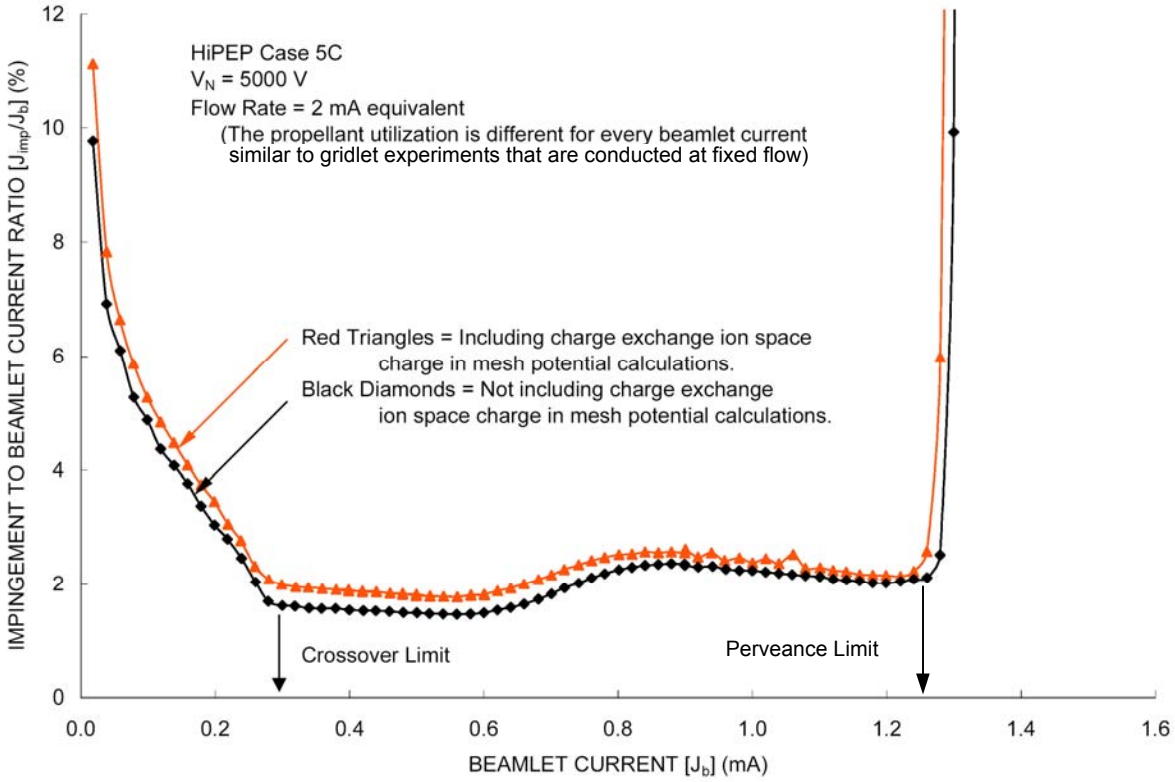

Fig. 11b ffx generated impingement current plot including effect of charge-exchange ion production processes.

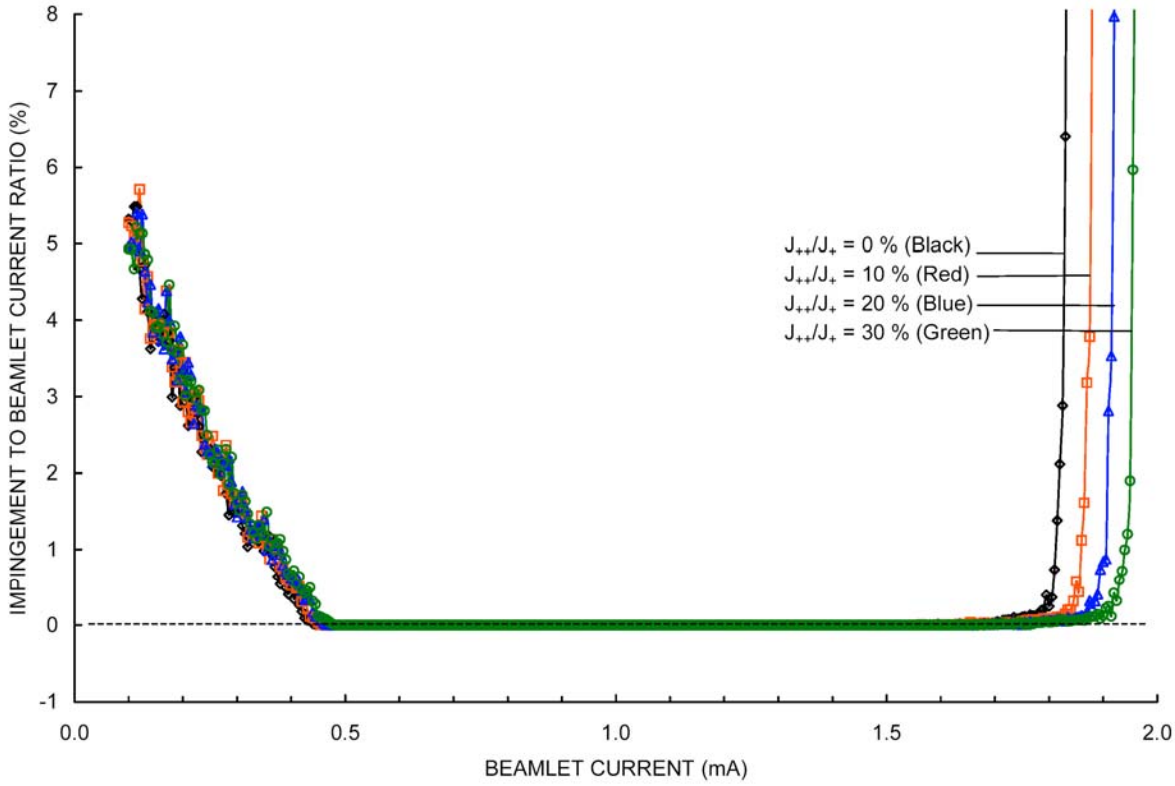

Fig. 12 Effect of doubles-to-singles ratio on impingement current data as determined using ffx. (Case 5C)

One can reduce data from simulations and experiment to determine the sensitivity of impingement limit data on a given parameter. This is accomplished by first obtaining the impingement current limits at a given operating condition and at operating conditions that correspond to slightly different values of a given parameter. When one divides the new impingement limits by the nominal limit and plots these values against the normalized parameter being studied, the resulting slope of this plot describes the sensitivity in units of %/%. The sensitivity is typically referred to as the percent change in the dependent parameter due to a given percent change in an independent parameter. As a mathematical example of this technique, consider Eq. (1) where the dependence of perveance limit on total voltage is given as $V_T^{3/2}$. The sensitivity is given as

$$
\begin{aligned}
s &= \left.\frac{\partial J_{b,pl}}{\partial V_T}\right|_{V_T = V_{T\,nom}} \cdot \frac{V_{T\,nom}}{J_{b,pl\,nom}} \\
&= 3/2 \; \frac{\pi \varepsilon_o}{9} \sqrt{\frac{2q}{m}} \, V_{T\,nom}^{1/2} \, \frac{d_s^2}{\ell_e^2} \cdot V_T \cdot \frac{1}{\frac{\pi \varepsilon_o}{9} \sqrt{\frac{2q}{m}} \, V_{T\,nom}^{3/2} \, \frac{d_s^2}{\ell_e^2}} \\
&= 3/2 \;\; \%/\%
\end{aligned}
$$

The subscript designation "nom" refers to the nominal value of that parameter, and the other parameters in Eq. (3) were defined earlier. If one were to perform the same operations on Eq. (1) with respect to ℓ_e for example, a sensitivity of -2 %/% would be obtained. Sensitivity calculations were performed on ffx simulation results and gridlet experimental data to determine the sensitivity of crossover and perveance limits on many parameters. The results of this effort are shown in Table 2 where the sensitivities are ranked from strongest to weakest.

Table 2 Sensitivity data from ffx modeling and experimental measurements (ranked highest to lowest).

Parameter	Description	Perveance Limit Sensitivity (%/%)	Source for Sensitivity Calc.
ℓ_e	Effective acceleration length	-2.22	ffx simulation Case 5A
"	" "	-2.29	Experiment Case 5B
V_T	Total voltage	1.48	ffx simulation Case 5A
"	" "	1.54 ± 0.12	Experiment Case 5B
"	" "	1.56	Experiment Case 5A
d_a	Accel hole diameter	0.97	ffx simulation Case 5A
"	" "	0.63	Experiment Case 5A
t_s	Screen grid thickness	-0.25	ffx simulation Case 5A
J_+/J_b	Single ion content	-0.22	ffx simulation Case 5C
V_{dp}	Discharge plasma potential	-0.086	ffx simulation Case 5C
ℓ_{cc}	Hole-to-hole spacing	0.052	ffx simulation Case 5C
t_a	Accel grid thickness	-0.0075	ffx simulation Case 5A
T_e	Discharge electron temp.	0.0025	ffx simulation Case 5C

Parameter	Description	Crossover Limit Sensitivity (%/%)	Source for Sensitivity Calc.
V_T	Total voltage	1.95	ffx simulation Case 5A
"	" "	1.37	Experiment Case 5B
"	" "	1.46	Experiment Case 5A
d_a	Accel hole diameter	-1.73	ffx simulation Case 5A
		-1.44	Experiment Case 5A
ℓ_e	Effective acceleration length	-1.34	ffx simulation Case 5A
"	" "	-0.49	Experiment Case 5B
t_s	Screen grid thickness	1.20	ffx simulation Case 5A
ℓ_{cc}	Hole-to-hole spacing	-0.59	ffx simulation Case 5A
t_a	Accel grid thickness	0.52	ffx simulation Case 5A
V_{dp}	Discharge plasma potential	-0.40	ffx simulation Case 5A
J_+/J_b	Single ion content	-0.0535	ffx simulation Case 5C
T_e	Discharge electron temp.	0.00	ffx simulation Case 5C

In general, good agreement was observed between experimental data and ffx simulations, and a more detailed discussion of comparisons between the two is given by Farnell.[5] Briefly, the largest difference corresponds to the crossover limit sensitivity on the effective acceleration length, ℓ_e, where experiment suggests an inverse square root dependence and numerical simulation suggests an inverse ~3/2 power dependence. In regard to perveance limit sensitivities, most are very similar between experiment and simulation, and no smoking gun was found to explain the differences observed at ultra-low flow operation (see Fig. 10).

Figure 13 contains backstreaming margin data obtained using the ffx program for Case 5C geometry, but at a grid-to-grid spacing that is only 9.09 rather than 11.36 (relative to NSTAR spacing as listed in Table 1). At the tighter spacing, the saddlepoint potential[5] is nearly at 0 V for a beamlet current of 0.7 mA (note that the peak HiPEP beamlet current is about 1 mA). The saddlepoint potential represents the minimum resistance for preventing a beam plasma electron from backstreaming, and saddlepoint potential values close to the beam plasma potential (assumed to be +10 V) suggest that very little margin exists before backstreaming will begin to occur. The same result is indicated in Fig. 7 where the backstreaming limit was interpolated to be ~620 V at a spacing of 9.09 and net accelerating voltage of 6.7 kV. As shown in Fig. 13, increasing the accelerator voltage magnitude by 100 V was found to increase the backstreaming margin by 85 V.

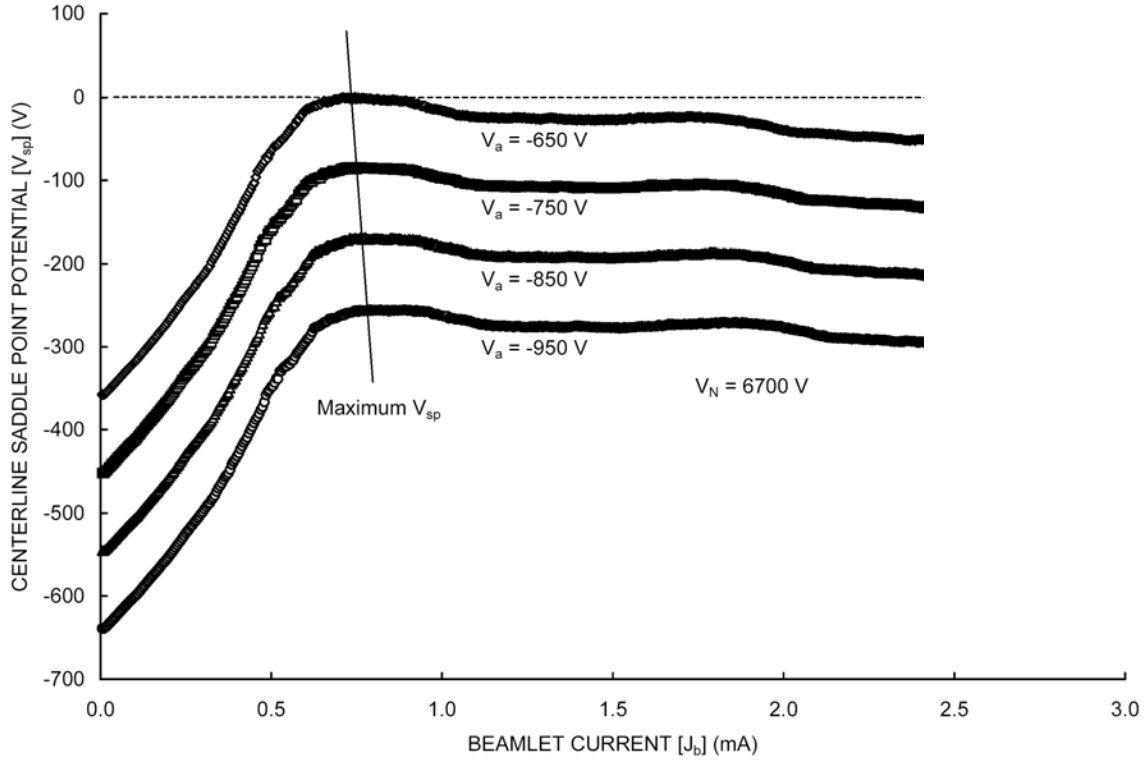

Fig. 13 Backstreaming voltage margins predicted from ffx numerical simulations. (Case 5A modified to have slightly smaller hole-to-hole spacing and significantly smaller grid-to-grid spacing)

IV. Conclusions

An experimental study of sub-scale High Power Electric Propulsion (HiPEP) ion optics designs proposed by the NASA Glenn Research Center was performed in which perveance and crossover beamlet current limits were identified over wide ranges of geometrical and operational conditions. Backstreaming voltage limits were measured for different grid spacing to help finalize selection of this parameter and for accel gridlets that were fabricated with progressively larger accel diameters to simulate the effects of accel barrel erosion over life. Numerical models of impingement current and electron backstreaming processes were observed to yield limits that agree well with experimental values, however, some differences were identified. In particular additional work is needed to bring numerical and experimental determined crossover limits into better agreement. Currently, numerical predictions of crossover limits are lower than measured values. Experimental crossover data were reduced in an attempt to

identify dependencies on applied voltage and geometrical features. A dependence on total voltage to the 3/2 power was identified for crossover limit behavior. In addition, experimental crossover limits appear to vary with accelerator hole diameter raised to the -1.5 power and grid gap raised to the -0.5 power. Good agreement was observed between experimentally measured and numerically estimated (via ffx) sensitivities, which suggests that most of the essential physics has been correctly included in the ffx model.

References

[1] P.J. Wilbur, J. Miller, C.C. Farnell, and V.K. Rawlin, "A Study of High Specific Impulse Ion Thruster Optics," IEPC-01-098, 27th International Electric Propulsion Conference, Pasadena, CA, 2001.

[2] J.R. Brophy, J.E. Polk, and L.C. Pless, "Test-to-Failure of a Two-Grid, 30-cm-dia. Ion Accelerator System," IEPC-93-172, 23rd International Electric Propulsion Conference, Seattle, WA, 1993.

[3] J.D. Williams, D.M. Goebel, and P.J. Wilbur, "A Model of Electron Backstreaming in Ion Thrusters," AIAA-2003-4560, 39th Joint Propulsion Conference, Huntsville, AL, 2003.

[4] J.E. Foster, et al, "An Overview of the High Power Electric Propulsion (HiPEP) Project ," AIAA-2004-3453, 40th Joint Propulsion Conference, Fort Lauderdale, FL, 2004.

[5] C.C. Farnell, "Numerical Simulation of HiPEP Ion Optics," AIAA-2004-3818, 40th Joint Propulsion Conference, Fort Lauderdale, FL, 2004.

[6] J.D. Williams, D.M. Laufer, and P.J. Wilbur, "Experimental Performance Limits on High Specific Impulse Ion Optics," IEPC-03-128, 28th International Electric Propulsion Conference, Toulouse France, March 2003.

[7] P.J. Wilbur, "Limits on High Specific Impulse Ion Thruster Operation," AIAA-2004-4106, , 40th Joint Propulsion Conference, Fort Lauderdale, FL, 2004.

REPORT DOCUMENTATION PAGE

Form Approved
OMB No. 0704-0188

1. AGENCY USE ONLY (*Leave blank*)	2. REPORT DATE	3. REPORT TYPE AND DATES COVERED
	January 2006	Final Contractor Report

4. TITLE AND SUBTITLE

HiPEP Ion Optics System Evaluation Using Gridlets

5. FUNDING NUMBERS

WBS–22–319–20–B2
NNC04GB20G

6. AUTHOR(S)

John D. Williams, Cody C. Farnell, D. Mark Laufer, and Rafael A. Martinez

7. PERFORMING ORGANIZATION NAME(S) AND ADDRESS(ES)

Colorado State University
1 Colorado State
Fort Collins, Colorado 80523–0001

8. PERFORMING ORGANIZATION REPORT NUMBER

E–14745

9. SPONSORING/MONITORING AGENCY NAME(S) AND ADDRESS(ES)

National Aeronautics and Space Administration
Washington, DC 20546–0001

10. SPONSORING/MONITORING AGENCY REPORT NUMBER

NASA CR—2006-213298
AIAA–2004–2814

11. SUPPLEMENTARY NOTES

Prepared for the 40th Joint Propulsion Conference and Exhibit cosponsored by the AIAA, ASME, SAE, and ASEE, Fort Lauderdale, Florida, July 11–14, 2004. Project Manager, John Foster, Power and On–Board Propulsion Technology Division, NASA Glenn Research Center, organization code 5430, 216–433–6131.

12a. DISTRIBUTION/AVAILABILITY STATEMENT

Unclassified - Unlimited
Subject Category: 20 Distribution: Nonstandard

Available electronically at http://gltrs.grc.nasa.gov

This publication is available from the NASA Center for AeroSpace Information, 301–621–0390.

12b. DISTRIBUTION CODE

13. ABSTRACT ***(Maximum 200 words)***

Experimental measurements are presented for sub-scale ion optics systems comprised of 7 and 19 aperture pairs with geometrical features that are similar to the HiPEP ion optics system. Effects of hole diameter and grid-to-grid spacing are presented as functions of applied voltage and beamlet current. Recommendations are made for the beamlet current range where the ion optics system can be safely operated without experiencing direct impingement of high energy ions on the accelerator grid surface. Measurements are also presented of the accelerator grid voltage where beam plasma electrons backstream through the ion optics system. Results of numerical simulations obtained with the ffx code are compared to both the impingement limit and backstreaming measurements. An emphasis is placed on identifying differences between measurements and simulation predictions to highlight areas where more research is needed. Relatively large effects are observed in simulations when the discharge chamber plasma properties and ion optics geometry are varied. Parameters investigated using simulations include the applied voltages, grid spacing, hole-to-hole spacing, doubles-to-singles ratio, plasma potential, and electron temperature; and estimates are provided for the sensitivity of impingement limits on these parameters.

14. SUBJECT TERMS	15. NUMBER OF PAGES
Ion propulsion; Ion optics	21
	16. PRICE CODE

17. SECURITY CLASSIFICATION OF REPORT	18. SECURITY CLASSIFICATION OF THIS PAGE	19. SECURITY CLASSIFICATION OF ABSTRACT	20. LIMITATION OF ABSTRACT
Unclassified	Unclassified	Unclassified	